TRANSPORT-DISSIPATION ANALYTICAL SOLUTIONS TO THE $E-\epsilon$ TURBULENCE MODEL AND THEIR ROLE IN PREDICTIONS OF THE NEUTRAL ABL

A. FRANK R. FREEDMAN* and B. MARK Z. JACOBSON
Environmental Fluid Mechanics Laboratory, Department of Civil and Environmental Engineering, Stanford University, U.S.A.

(Received in final form 22 May 2001)

Abstract. $E-\epsilon$ turbulence model predictions of the neutral atmospheric boundary layer (NABL) are reinvestigated to determine the cause for turbulence overpredictions found in previous applications. Analytical solutions to the coupled E and ϵ equations for the case of steady balance between transport and dissipation terms, the dominant balance just below the NABL top, are derived. It is found that analytical turbulence profiles laminarize at a finite height only for values of closure parameter ratio $\kappa \equiv c_{\epsilon 2}\sigma_\epsilon/\sigma_e$ equal to or slightly greater than one, with laminarization as $z \to \infty$ for greater κ. The point $\kappa = 2$ is additionally found that where analytical turbulent length scale (l) profiles made a transition from ones of decreasing ($\kappa < 2$) to increasing ($\kappa > 2$) values with height. Numerically predicted profiles near the NABL top are consistent with analytical findings. The height-increasing values of l predicted throughout the NABL with standard values of closure parameters thus appear a consequence of $\kappa \approx 2.5$ (> 2), implied by these values ($c_{\epsilon 2} = 1.92$, $\sigma_\epsilon = 1.3$, $\sigma_e = 1$). Comparison of numerical predictions with DNS data shows that turbulence overpredictions obtained with standard-valued parameters are rectified by resetting σ_ϵ and σ_e to $\approx$1.1 and 1.6, respectively, giving, with $c_{\epsilon 2} = 1.92$, $\kappa \approx 1.3$, and laminarization of the NABL's capping transport-dissipation region at a finite height.

Keywords: $E-\epsilon$ model, Neutral atmospheric boundary layer, Turbulence parameterization.

1. Introduction

In turbulence models for meso- and large-scale Reynolds-averaged meteorological prediction, there is strong motivation to supplant typically used algebraic length scale formulations with a more generally applicable transport equation for the length or other turbulence 'scale' quantity. The most common quantity for engineering flow computation is the dissipation rate, ϵ, of turbulent kinetic energy, E. Unlike the E-equation, however, direct closure of source and sink terms in the theoretical transport equation for ϵ is intractable, and a modelled equation, with source and sink terms analogous to those in the E-equation, is employed. Closure parameter values in this equation (hereafter referred to as the 'ϵ-equation') are empirically determined to give accurate predictions of various engineering benchmark flows. Integration of the E- and ϵ-equations then supplies

* E-mail: freedman@stanford.edu

Boundary-Layer Meteorology **102:** 117–138, 2002.

the length scale, $l \propto E^{3/2}/\epsilon$, necessary to compute eddy viscosities and diffusivities for turbulence fluxes in the mean equations. In this paper, we reinvestigate the predictive inaccuracies of this approach when applied to the one-dimensional, horizontally homogeneous, barotropic, neutrally-stratified atmospheric boundary layer (NABL).

Previous applications of the ϵ-equation to the NABL (Detering and Etling, 1985; Duynkerke, 1988; Huang and Raman, 1991; Andrén, 1991; Koo and Reible, 1995; Apsley and Castro, 1997; Xu and Taylor, 1997) yielded a more turbulent and deep boundary layer than suggested by field data. In addition, l values increased with height throughout the boundary layer, at odds with popular Blackadar (1962) algebraic formulations in which a constant value is approached with height. Although small amounts of static stability in field data used for evaluation (see Duynkerke, 1988 for a discussion) prevent unequivocal statement of model inaccuracy, most of the previous investigators modified the ϵ-equation by implementing in various ways an additional production mechanism in the equation (or its effects elsewhere in the model) to lower model-predicted values of l aloft and thereby bring predicted turbulence levels and boundary-layer depths to better agreement with field measurements. Here, we present analytical and numerical work that i) links the need for additional ϵ-production to model inability to produce laminarization at a finite height of the NABL's capping region of transport-dissipation turbulence energy balance and ii) demonstrates rectification of this inability and of associated turbulence overpredictions by alteration of key closure parameter values from those standardly employed in engineering flow computation.

2. Basic Equations

The NABL equations for the mean horizontal streamwise (in the direction of the geostrophic wind) and cross-stream (perpendicular and to the left of the geostrophic wind) velocity components, U and V, respectively, are

$$\frac{\partial U}{\partial t} = fV - \frac{\partial \overline{uw}}{\partial z}, \tag{1}$$

$$\frac{\partial V}{\partial t} = -f(U - G) - \frac{\partial \overline{vw}}{\partial z}, \tag{2}$$

where G is the geostrophic wind speed (independent of height as per the barotropic assumption), f is the Coriolis parameter, $\overline{uw}$ and $\overline{vw}$ are the u and v components of the vertical turbulent momentum flux (Reynolds stress), respectively, t is time and z is height. In the $E - \epsilon$ model, $\overline{uw}$ and $\overline{vw}$ are represented by flux-gradient relationships

$$\overline{uw} = -K_m \frac{\partial U}{\partial z}, \tag{3}$$

$$\overline{vw} = -K_m \frac{\partial V}{\partial z}, \tag{4}$$

with eddy viscosity, K_m, modelled as

$$K_m = c_\mu E^2/\epsilon. \tag{5}$$

The following transport equations for turbulent kinetic energy (TKE), E, and its dissipation rate, ϵ, close the model,

$$\frac{\partial E}{\partial t} - \frac{\partial}{\partial z}\left(\frac{K_m}{\sigma_e}\frac{\partial E}{\partial z}\right) = -\overline{uw}\frac{\partial U}{\partial z} - \overline{vw}\frac{\partial V}{\partial z} - \epsilon, \tag{6}$$

$$\frac{\partial \epsilon}{\partial t} - \frac{\partial}{\partial z}\left(\frac{K_m}{\sigma_\epsilon}\frac{\partial \epsilon}{\partial z}\right) = -\frac{c_{\epsilon 1}}{\tau}\left(\overline{uw}\frac{\partial U}{\partial z} + \overline{vw}\frac{\partial V}{\partial z}\right) - \frac{c_{\epsilon 2}}{\tau}\epsilon, \tag{7}$$

where $\tau \equiv E/\epsilon$. The determination of values for closure parameters c_μ, $c_{\epsilon 1}$, $c_{\epsilon 2}$, σ_ϵ and σ_e is discussed below. Of interest here is the steady solution to (1)-(7) subject to appropriate boundary conditions (Section 4.1).

The combination of the first two terms on the right side of (6) is the TKE shear production rate and the second term on the left side represents TKE turbulent transport. ϵ-equation (7), a modelled form of the theoretical equation (Tennekes and Lumley, 1972) is a dimensionally consistent analogy to (6). Rationale and additional ideas behind the modelling assumptions implicit in (7) are discussed in a number of literature (e.g., Jones and Launder, 1972; Andrén, 1991; Speziale and Bernard, 1992; Speziale and Gatski, 1996; Xu and Taylor, 1997; Wilcox, 1998).

The value of c_μ is set by matching (3) and (5) to a classical neutral surface layer. Specifically, aligning the u-coordinate with the direction of the surface shear stress, and inserting (5) into (3) with $\partial U/\partial z = u_\star/kz$, $\epsilon = u_\star^3/kz$ and $\overline{uw} = -u_\star^2$ (where $u_\star$ is the surface friction velocity and k is the Von Karman constant), gives

$$c_\mu^{1/2} = u_\star^2/E \equiv \beta_0, \tag{8}$$

with β_0 amenable to laboratory and/or micrometeorological measurement. The value of $c_{\epsilon 2}$ is set to be consistent with experimentally determined decay rates of unsheared isotropic turbulence. Inserting (8) and the above neutral surface-layer expressions into the steady form of (7) gives a third condition,

$$k^2 = \sigma_\epsilon c_\mu^{1/2}(c_{\epsilon 2} - c_{\epsilon 1}). \tag{9}$$

With values of c_μ and $c_{\epsilon 2}$ determined as above and arbitrarily setting $\sigma_e = 1$, the engineering values of $c_{\epsilon 1}$ and σ_ϵ were then determined by optimizing agreement with experimentally determined spreading rates of a plane mixing layer while simultaneously satisfying (9) with $k \approx 0.4$. Determined in this manner, the 'standard' values are

$$[c_\mu, c_{\epsilon 1}, c_{\epsilon 2}, \sigma_\epsilon, \sigma_e] = [0.09, 1.44, 1.92, 1.3, 1.0]. \tag{10}$$

Inserting these into (9) gives $k \approx 0.43$. Further details on this calibration procedure are given in Durbin and Pettersson-Reif (2001).

For later reference, we note that (5) can be represented in terms of l through

$$K_m = c_\mu^{1/4} l E^{1/2}, \tag{11}$$

with

$$l = c_\mu^{3/4} E^{3/2} / \epsilon. \tag{12}$$

The partitioning of c_μ between (11) and (12) is chosen so that $l = kz$ in a classical neutral surface layer, which can be checked by inserting $\epsilon = u_\star^3 / kz$ and, from (8), $E = c_\mu^{-1/2} u_\star^2$ into (12). This ensures consistency with commonly used algebraic l formulations (e.g., Blackadar, 1962).

3. Transport-Dissipation Solutions

In this section, we derive a set of analytical solutions to (6) and (7) for the case of steady balance between transport and dissipation terms. Analytical, field, large-eddy simulation (LES) and direct numerical simulation (DNS) studies (Deaves, 1981; Mason and Thomson, 1987; Coleman et al., 1990; Grant, 1992) support the dominance of this TKE balance in the weakly turbulent, nearly geostrophic, shearless region just below the NABL top. The analytical solutions may thus be relevant to the full model's solutions (i.e., with all terms present) in the region, and will be used to gain insight into turbulence profiles predicted from full-model numerical integrations discussed in Section 4.

The lower boundary of the analytical domain is an arbitrary height $z = h_B$, where $E = E_B$ and $\epsilon = \epsilon_B$ are presumed known. In reference to the NABL, this height can be thought near $z = h_\tau$, at which the magnitude of the vertical turbulent momentum flux falls to 5% of its surface value. Two general types of solutions are derived. In the first, E and ϵ laminarize (equal zero) at a distinct height ('edge') $z = h_L$ above h_B. In the second, E and ϵ laminarize as $z \to \infty$, and there is no distinct edge to the turbulent region above h_B.

3.1. Power-law solution with an edge (PL-E)

The solution type sought here was assumed in the analytical work of Deaves (1981). We first make the coordinate transformation

$$\eta \equiv \frac{h_L - z}{\Delta h}, \tag{13}$$

where $\Delta h \equiv h_L - h_B$. Assuming steady transport-dissipation balances in (6) and (7) and substituting (5) as well as, from (13), $dz = -\Delta h d\eta$ leads to

$$\frac{c_\mu}{\sigma_e \Delta h^2} \frac{d}{d\eta} \left(\frac{E^2}{\epsilon} \frac{dE}{d\eta} \right) = \epsilon, \tag{14}$$

$$\frac{c_\mu}{\sigma_\epsilon \Delta h^2}\frac{d}{d\eta}\left(\frac{E^2}{\epsilon}\frac{d\epsilon}{d\eta}\right) = c_{\epsilon 2}\frac{\epsilon^2}{E}. \tag{15}$$

We seek power-law solutions to (14) and (15) of the form $E = E_B\eta^p$ and $\epsilon = \epsilon_B\eta^q$ satisfying the upper boundary conditions

$$E = 0,\ dE/d\eta = 0 \ \text{ at } \ \eta = 0, \tag{16}$$

$$\epsilon = 0,\ \ d\epsilon/d\eta = 0 \ \text{ at } \ \eta = 0, \tag{17}$$

and hence $p > 1$ and $q > 1$. Inserting the solutions into (14) and (15) gives

$$\left(\frac{c_\mu}{\sigma_e}\right)p(3p - q - 1)\eta^{3p-2q-2} = \frac{\epsilon_B^2\Delta h^2}{E_B^3}, \tag{18}$$

$$\left(\frac{c_\mu}{\sigma_\epsilon c_{\epsilon 2}}\right)q(2p - 1)\eta^{3p-2q-2} = \frac{\epsilon_B^2\Delta h^2}{E_B^3}. \tag{19}$$

Since the right sides of (18) and (19) are not functions of η, the condition from the left side $3p - 2q - 2 = 0$ must be satisfied, and hence

$$q = 3p/2 - 1. \tag{20}$$

Inserting (20) with the proposed solutions into (5) and (12) then gives

$$K_m \sim \eta^{p/2+1}, \tag{21}$$

$$l \sim \eta, \tag{22}$$

and hence l *decreases* with height to zero at h_L, as do E and ϵ. Inserting (20) into (18) and (19) and equating the resulting expressions then leads to

$$(6 - 3\kappa)p^2 - 7p + 2 = 0, \tag{23}$$

where

$$\kappa \equiv \frac{c_{\epsilon 2}\sigma_\epsilon}{\sigma_e}. \tag{24}$$

It can be checked that solutions for p and q satisfying (16) and (17) are obtained from the positive solution branch of (23). We additionally stipulate:

1. $\epsilon \to 0$ as fast or faster than $E \to 0$ as $\eta \to 0$ ($q \geq p$).
2. Values of p and q are O(1).

The first is based on classical arguments of TKE decay, whereby small, dissipative eddies are extinguished before large, energetic eddies. The second reflects efforts to avoid the singular point $\kappa = 2$ in the positive solution branch of (23), for which $p = \infty$. It can be verified that solutions satisfying (16), (17) and these additional constraints exist for

$$1 \leq \kappa \leq \kappa_A, \tag{25}$$

where $\kappa_A < 2$ is a loosely defined unknown value of κ above which p and q exceed O(1). From (20) and the positive solution branch of (23), it can be checked that (25) corresponds to $2 \leq p \leq p_A$ and $2 \leq q \leq q_A$, where p_A and q_A ($> p_A$) are values of p and q, respectively, at κ_A.

3.2. Power-law solution without an edge (PL-NE)

The solution shown here was also derived by Briggs et al. (1996). We first make the coordinate transformation

$$\hat{z} \equiv z/h_B. \tag{26}$$

Power-law solutions of the form $E = E_B \hat{z}^p$ and $\epsilon = \epsilon_B \hat{z}^q$ are then sought subject to the upper boundary conditions

$$E \to 0, \ \hat{z} \to \infty, \tag{27}$$

$$\epsilon \to 0, \ \hat{z} \to \infty, \tag{28}$$

and hence $p < 0$ and $q < 0$. Inserting these solutions into (6) and (7) under steady transport-dissipation balance then yields expressions analogous to (18) and (19) with the replacements $\hat{z}$ for η and h_B for Δh. Equations (20) and (23) for q and p, respectively, thus still hold. Solutions for l and K_m are analogous to (21) and (22),

$$K_m \sim \hat{z}^{p/2+1}, \tag{29}$$

$$l \sim \hat{z}, \tag{30}$$

and therefore, contrary to the PL-E solution, l *increases* with height throughout the analytical domain. Valid solutions for p and q are those satisfying (27), (28) and the constraints

1. $K_m \to 0$ as $\hat{z} \to \infty$.
2. Values of p and q are O(1).

The reasoning for the second is stated above in connection with the PL-E solution. The first is based on physical considerations, and from (29) implies $p < -2$.

Solutions satisfying these conditions result from the positive solution branch of (23) provided

$$\kappa_B \leq \kappa < 10/3, \tag{31}$$

where κ is defined by (24) and $\kappa_B > 2$ is a loosely defined unknown value of κ below which p and q exceed O(1). From (20) and the positive solution branch of (23), it can be checked that (31) corresponds to $p_B \leq p \leq -2$ and $q_B \leq q \leq -4$, where p_B and q_B ($< p_B$) are the values of p and q, respectively, at κ_B.

3.3. Exponential solution without an edge (EXP-NE)

We first make the coordinate transformation

$$z^\star \equiv (z - h_B)/\Delta h^\star, \tag{32}$$

where $\Delta h^\star \equiv h_L^\star - h_B$ and $h_L^\star$ is a scale height of exponential turbulence decay. Solutions of the form $E = E_B e^{-pz^\star}$ and $\epsilon = \epsilon_B e^{-qz^\star}$ are then sought subject to the upper boundary conditions

$$E \to 0, \;\; z^\star \to \infty, \tag{33}$$

$$\epsilon \to 0, \;\; z^\star \to \infty, \tag{34}$$

and hence $p > 0$ and $q > 0$. Inserting these solutions into (6) and (7) under steady transport-dissipation balance yields

$$\left(\frac{c_\mu}{\sigma_e}\right) p(3p - q) e^{-(3p-2q)z^\star} = \frac{(\epsilon_B \Delta h^\star)^2}{E_B^3}, \tag{35}$$

$$2\left(\frac{c_\mu}{c_{\epsilon 2}\sigma_\epsilon}\right) pq e^{-(3p-2q)z^\star} = \frac{(\epsilon_B \Delta h^\star)^2}{E_B^3}. \tag{36}$$

Since the right sides of (35) and (36) are not functions of $z^\star$, the condition $3p - 2q = 0$ from the left side must be satisfied, and hence

$$q = 3p/2. \tag{37}$$

Inserting this and the proposed solutions into (5) and (12) then gives

$$K_m \sim e^{-pz^\star/2}, \tag{38}$$

$$l \sim constant. \tag{39}$$

The fact that l is constant suggests the EXP-NE solution as intermediary between the PL-E and PL-NE solutions, for which l decreases and increases with height, respectively. Inserting (37) into (35) and (36) and equating the resulting expressions then leads to cancellation of p, collapsing the final expression to

$$\kappa = 2, \tag{40}$$

where κ is defined by (24). An exponentially decaying solution therefore exists only for $\kappa = 2$, with p and q undeterminable by this analysis method. It is interesting, and probably not a coincidence, that $\kappa = 2$ corresponds to a singularity in the PL-E and PL-NE solutions. The EXP-NE solution thus seems that asymptotically approached in the PL-E and PL-NE cases as $\kappa \to 2$ from the positive and negative directions, respectively. This relationship among the solutions is consistent with the intermediary behaviour of the EXP-NE solution with respect to l.

3.4. Summary of solutions

A qualitative summary of the analytical solutions is shown in Figure 1. Power-law solutions with (PL-E) and without (PL-NE) an edge exist for κ ranges (25) and (31), respectively. An exponential solution (EXP-NE) exists for $\kappa = 2$. For $\kappa_A \leq \kappa < 2$ and $2 < \kappa \leq \kappa_B$, 'mixed' PL-E/EXP-NE and PL-NE/EXP-NE solutions, respectively, are proposed, representing hybrids of the exponential and power-law types. These mixed solutions are not derived above, but are proposed intuitively from matching the EXP-NE to the PL-E and the EXP-NE to the PL-NE solutions as $\kappa \to 2$ from below and above, respectively. In the PL-E solution, l *decreases* with height towards zero at $z = h_L$. In the PL-NE solution, l *increases* with height. Finally, in the EXP-NE solution, l is *constant*. The point $\kappa = 2$, at which the EXP-NE solution is valid, thus also represents that at which l transitions from a height-decreasing ($\kappa < 2$) to a height-increasing profile ($\kappa > 2$). The regions $\kappa < 1$ and $\kappa > 10/3$ give unphysical solutions for reasons given above and in the figure.

4. Numerical Computations

In this section, we discuss the results of numerical computations of the NABL performed over a range of κ. The goals are a) to check the relevance of the analytical solutions derived in Section 3 to the full model's solutions near the NABL top and b) to examine the effect of κ on the behaviour and accuracy of model predictions.

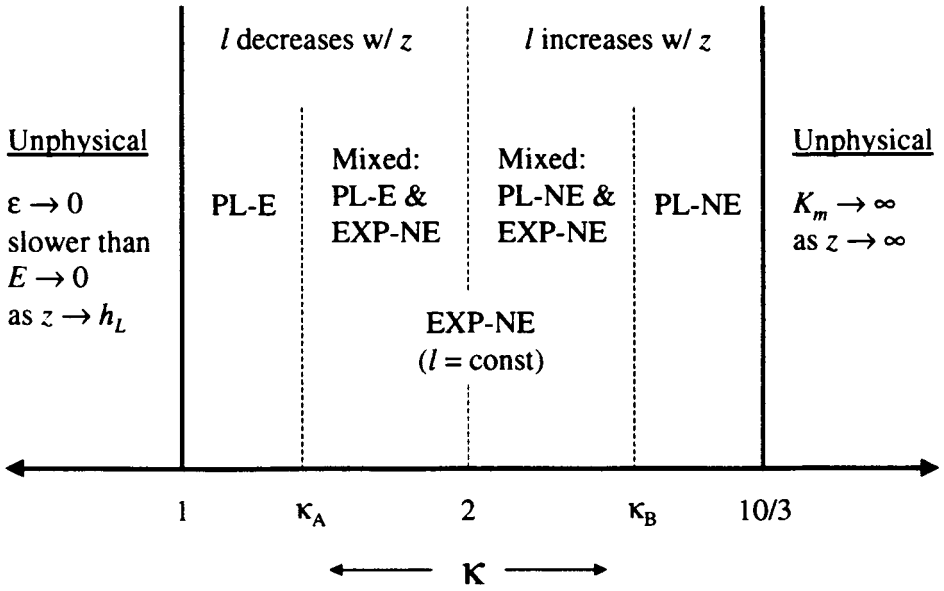

Figure 1. Qualitative summary of $E - \epsilon$ model transport-dissipation analytical solutions. Solution types plotted versus $\kappa \equiv c_{\epsilon 2}\sigma_\epsilon/\sigma_e$. Abbreviations and further explanation given in text.

4.1. METHODOLOGY

The steady solution to (1)–(7) is obtained by numerically solving the unsteady forms of these equations to convergence over eight inertial periods (where the inertial period equals $2\pi/|f|$). Variables are held on a staggered grid (mean velocities at layer midpoints and turbulence quantities at the levels), with central differencing used to compute vertical derivatives. Roughly 150 vertical levels are employed from the surface ($z = 0$) to the computational domain top $z_t = 37.5$ km. The lowest grid level is at $z = 100z_0$, where z_0 is the surface roughness length, with the spacing of higher levels stretched so that $\Delta z \approx 200$ m at $z \approx 5$ km. This places roughly 120 layers in the region $z < 5$ km, where essentially all boundary-layer structure exists among the computed NABLs.

Lower boundary conditions on (1) and (2) are obtained by computing the u and v components, $\tau_{u,0} \equiv (\overline{uw})_0$ and $\tau_{v,0} \equiv (\overline{vw})_0$, respectively, of the surface Reynolds stress. This is done by inverting the classical surface-layer logarithmic mean velocity profile expression to compute $u_\star$,

$$u_\star = \frac{kW_2}{\ln(h_2/z_0)}, \tag{41}$$

$$\tau_{u,0} = u_\star^2 \cos\alpha_0, \tag{42}$$

$$\tau_{v,0} = u_\star^2 \sin\alpha_0, \tag{43}$$

$$\alpha_0 = \tan^{-1}\left(\frac{V_2}{U_2}\right), \tag{44}$$

where U_2, V_2 and W_2 are the values of U, V and wind speed $W \equiv (U^2 + V^2)^{1/2}$, respectively, at h_2, the midpoint of the lowest computational grid layer, and α_0 is the surface layer mean wind direction relative to geostrophy. Equation (41) assumes a logarithmic mean velocity profile at $z = h_2$, an assumption valid provided $10 \lesssim h_2/z_0 \lesssim 150$ (Garratt, 1992). The height of the first grid level above the surface ($100z_0$, hence $h_2 = 50z_0$) is set to satisfy this condition. The lower boundary condition on (6) is defined by inverting (8)

$$E_0 = c_\mu^{-1/2} u_\star^2, \tag{45}$$

while for (7), the vertical flux of ϵ at h_2 is employed,

$$-\left(\frac{K_m}{\sigma_\epsilon}\frac{\partial \epsilon}{\partial z}\right)\Bigg|_{h_2} = \frac{u_\star^4}{\sigma_\epsilon h_2}, \tag{46}$$

derived by inserting $\epsilon = u_\star^3/kz$ and $K_m = u_\star kz$ into the left side of (46). For upper boundary conditions, $K_m = 0$ is specified at z_t and at the midpoint of the adjacent grid layer below. This specification, however, does not have appreciable effects since z_t is far above the disturbed region of the flow. Values $E = 1.0 \times 10^{-9}$ m^2 s^{-2} and $\epsilon = 1.0 \times 10^{-13}$ m^2 s^{-3} are specified in the undisturbed 'freestream' region above the computed NABL. Results, however, appear insensitive to the particular choice of these small, background values.

Cases RO5-RO8 (Table I) are performed with the standard parameter values (10) for different values of surface Rossby number $Ro \equiv G|f|/z_0$, so that basic model behaviour and consistency with Rossby-number similarity theory (Garratt, 1992) can first be evaluated. Cases K20-K10 are then performed for different κ. In these cases, G, f and z_0 are as in case RO6, and κ is varied by holding $c_{\epsilon 2}$ and σ_ϵ fixed (the value of σ_ϵ lowered slightly from the standard value to give, from (9), $k \approx 0.40$, more commonly accepted than $k \approx 0.43$ from the standard value) and raising σ_e.

Predictions are evaluated by comparing non-dimensionalized (by $u_\star$ and f) variables with DNS data of Coleman (1999, hereafter C99). Although the DNS was performed over a smooth surface and at a much lower value of bulk Reynolds number $Re \equiv GD/\nu$ (where $D = 2\nu/|f|$, with ν the molecular viscosity) than typical of the atmosphere, the utilized value of Re (1000) appears large enough for Reynolds-number (or analogously for a rough surface, Rossby-number) invariance of non-dimensionalized (as above) mean and large-scale turbulence profiles in the outer, rotationally-influenced region of the NABL to be satisfied to an adequate degree. This Re/Ro invariance ensures validity in comparing profiles computed by us over a rough surface at typically large atmospheric values of Ro with those

TABLE I

Computational cases.[a]

Case	G (ms^{-1})	f (s^{-1})	z_0 (m)	$Ro = G/\lvert f\rvert z_0$	σ_e	σ_ϵ	κ[b]	$\tilde{h}_\tau$[c]
RO5	5	1.263×10^{-4}	0.100	3.96×10^5	1.00	1.30	2.5	0.850
RO6	10	1.000×10^{-4}	0.100	1.00×10^6	1.00	1.30	2.5	0.852
RO7	5	7.292×10^{-5}	0.005	1.37×10^7	1.00	1.30	2.5	0.854
RO8	30	1.370×10^{-4}	0.002	1.09×10^8	1.00	1.30	2.5	0.854
K20	10	1.000×10^{-4}	0.100	1.00×10^6	1.07	1.11	2.0	0.721
K17	10	1.000×10^{-4}	0.100	1.00×10^6	1.25	1.11	1.7	0.681
K15	10	1.000×10^{-4}	0.100	1.00×10^6	1.43	1.11	1.5	0.650
K13	10	1.000×10^{-4}	0.100	1.00×10^6	1.64	1.11	1.3	0.623
K10	10	1.000×10^{-4}	0.100	1.00×10^6	2.13	1.11	1.0	0.580

[a] Symbols defined in text.
[b] $c_\mu = 0.09$, $c_{\epsilon 1} = 1.44$ and $c_{\epsilon 2} = 1.92$ for all cases.
[c] C99 DNS value, $\tilde{h}_\tau = 0.599$.

of the DNS computed over a smooth surface at relatively lower (with respect to typical atmospheric values) Re. Details regarding the Re-invariance of the DNS are given in C99.

DNS profiles of mean velocity and Reynolds stress components were obtained directly from Coleman. From these, we computed TKE shear production and used this to diagnosed the DNS K_m profile from

$$K_m = \frac{-\overline{uw}\,\partial U/\partial z - \overline{vw}\,\partial V/\partial z}{(\partial U/\partial z)^2 + (\partial V/\partial z)^2}. \tag{47}$$

The DNS l profile was then diagnosed from (11), making use of K_m from (47) and the DNS E profile, directly obtained. The validity of (47) rests on the suitability of the flux-gradient assumption underlying (3) and (4). Within the lower and middle portion ('bulk') of the NABL, where shear production and dissipation are in primary balance, the assumption is largely valid. In the upper NABL, however, where turbulent transport becomes important, the assumption is less valid, while in the freestream region above the NABL, diagnosed K_m and l values are not physical since Reynolds stresses and mean velocity gradients essentially vanish there. We thus view our diagnosed DNS profiles of K_m and l trustworthy only within the bulk of the NABL.

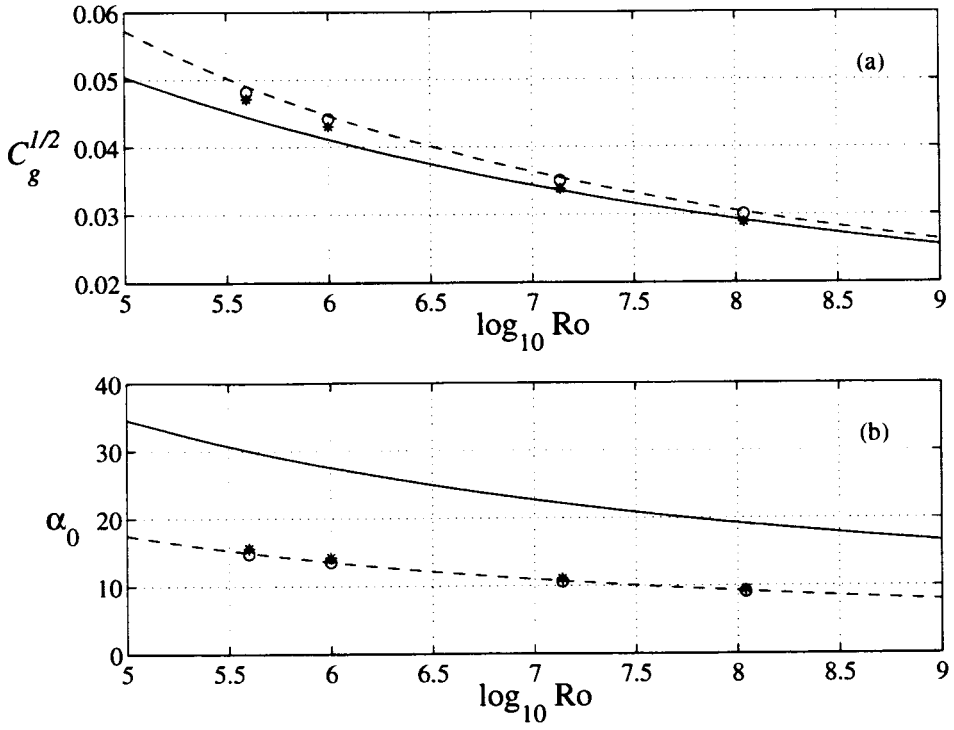

Figure 2. $E - \epsilon$ model predictions of (a) $C_g^{1/2} = u_\star/G$ and (b) α_0; 'o', standard-value cases RO5-RO8; '$*$', cases of same Ro, but with $\kappa = 1.3$ set as in case K13. Solid lines, (48) and (49) with $A_0 = 2$ and $B_0 = 4.1$; dashed lines, (48) and (49) with $A_0 = 2$ and $B_0 = 2.1$.

4.2. RESULTS

4.2.1. *Standard Parameter Values ($\kappa = 2.5$)*

We begin by evaluating predictions made with standard-valued parameters. Predictions of geostrophic drag coefficient, $C_g = u_\star^2/G^2$, and α_0 are shown in Figure 2 (symbol 'o'). Also shown are Rossby-number similarity expressions

$$C_g = \frac{k^2}{(\ln(Ro\, C_g) - A_0)^2 + B_0^2}, \tag{48}$$

$$\alpha_0 = \tan^{-1}\left(\frac{B_0\,\mathrm{sgn}(f)}{\ln(Ro\, C_g) - A_0}\right) \tag{49}$$

with $[A_0, B_0] = [2, 4.1]$, deduced from field measurements (Garratt, 1992), and with $[A_0, B_0] = [2, 2.1]$, deduced by C99 from his DNS. It is seen that predictions agree very well with curves formed from the DNS-deduced values of A_0 and B_0 but not well, particularly for α_0, onto curves formed from the field-deduced values. The lower C_g and higher α_0 in the field curves are most likely

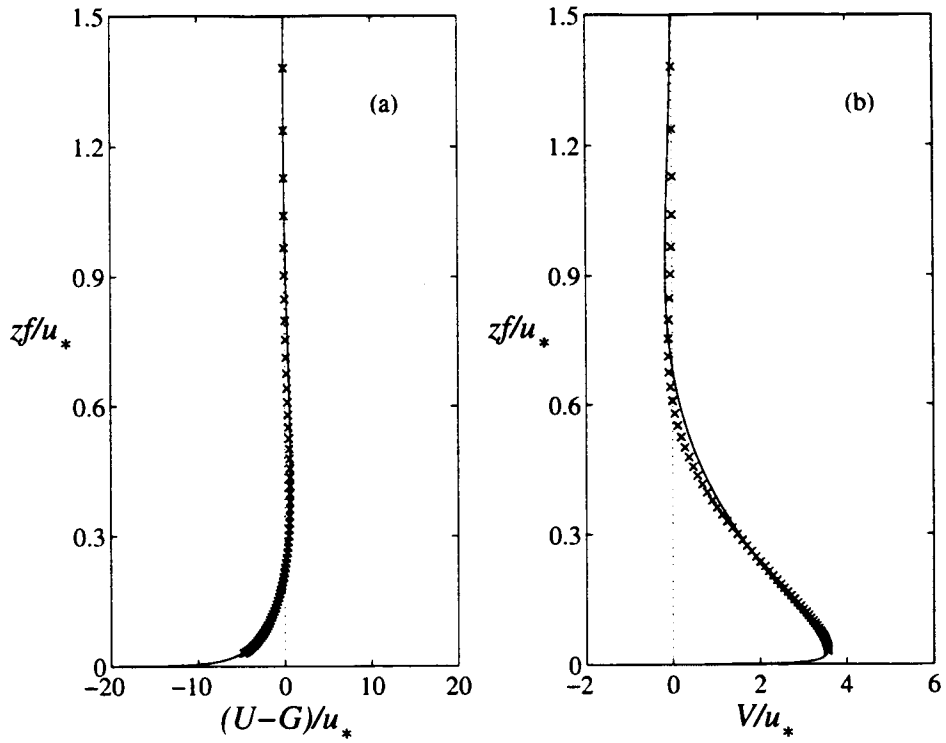

Figure 3. $E-\epsilon$ model predictions (solid line) of non-dimensional a) U and (b) V for case RO6. C99 DNS data for $\tilde{z} \equiv z|f|/u_\star > 0.03$ plotted as 'x'.

due to effects of stable stratification on field data. The fact that predictions fit well onto the shape of (48) and (49) suggests consistency with Rossby-number similarity, corroborated by the Ro-invariance of non-dimensional boundary-layer depth $\tilde{h}_\tau \equiv h_\tau|f|/u_\star$ (h_τ defined at beginning of Section 3) computed for each of the standard-value cases (Table I). The excellent agreement in value with the expressions using DNS-deduced values of A_0 and B_0 indicates that the model with standard-valued parameters accurately predicts mean momentum transport to the surface layer from higher levels of the NABL. This is further supported by the accuracy of mean velocity (Figure 3) and K_m (Figure 4a, solid line) predictions in the lower NABL ($\tilde{z} \equiv z|f|/u_\star \lesssim 0.1$), where the majority of mean momentum mixing takes place. The only appreciable inaccuracy in the lower NABL occurs for E (Figure 5, solid line), where the underprediction is due to an overly low value of E_0 imposed, through (45) and (8), by a value $\beta_0 = 0.30$ evidently higher than present in the DNS log-layer. We revisit this issue at the end of the next subsection.

Above the lower NABL, the standard values give significant overprediction of K_m (Figure 4a, solid line). Corresponding with this are overpredictions of E aloft (Figure 5, solid line) and a predicted value $\tilde{h}_\tau \approx 0.85$ greater than the DNS value $\tilde{h}_\tau \approx 0.60$ (Table I). These overpredictions, similar to those in previous applic-

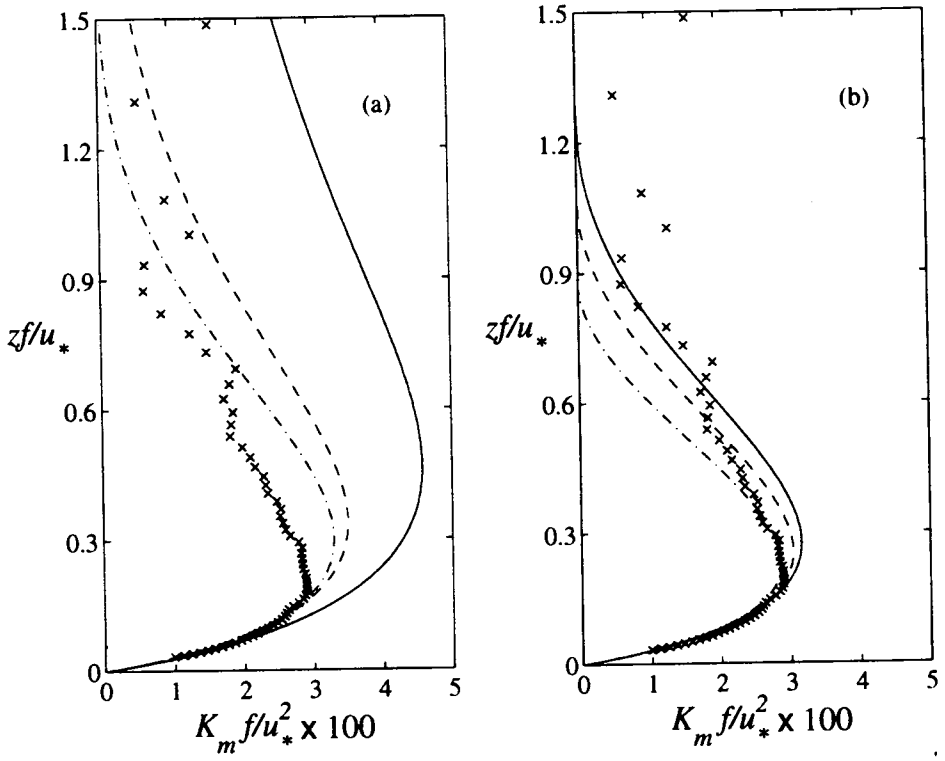

Figure 4. $E-\epsilon$ model predictions of non-dimensional K_m; (a) cases RO6 (solid), K20 (dashed), K17 (dashed-dot); (b) cases K15 (solid), K13 (dashed), K10 (dashed-dot). C99 DNS data for $\tilde{z} > 0.03$ plotted as 'x'.

ations using the standard values, do not adversely affect surface drag and mean velocity predictions in the lower NABL because mean velocity gradients aloft are small, and hence there is negligible contribution from aloft to the total mean momentum mixing within the boundary layer. Adverse effects on mean mixing throughout the boundary layer would, however, occur if appreciably strong mean gradients existed aloft, for example associated with pollution layers or different scalar concentrations between the boundary layer and free atmosphere.

4.2.2. *Modified Parameter Values (κ Varied)*

We begin examining the sensitivity of results to κ by checking relevance of the transport-dissipation analytical solutions to the region near the NABL top. Predicted profiles of TKE budget terms in the upper NABL (taken as the turbulent region above $\tilde{z} \approx 0.6$) are shown in Figure 6 for cases RO6 and K13. In case RO6 (Figure 6a), shear production clearly approaches zero with height faster than do transport and dissipation, leaving the latter two in primary balance. The transport-dissipation region in this case is elongated, extending far above that shown in the

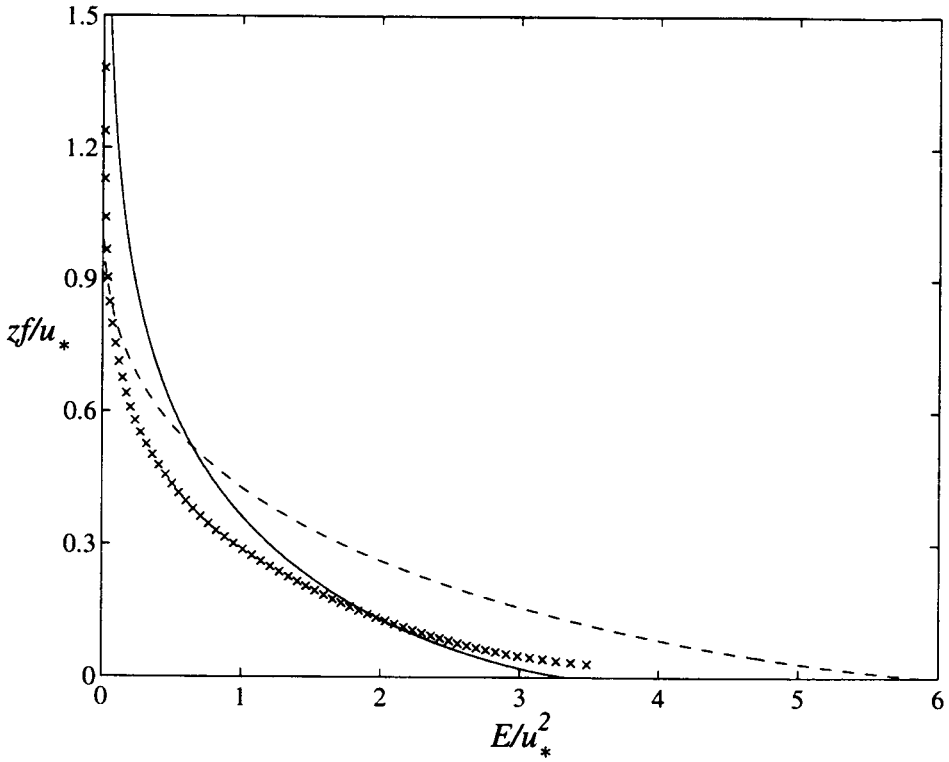

Figure 5. $E - \epsilon$ model predictions of non-dimensional E. Solid, case RO6; dashed, case with $c_\mu = 0.0289$ and $\kappa = 1.3$ (see text for details). C99 DNS data for $\tilde{z} > 0.03$ plotted as 'x'.

figure until eventually (at $\tilde{z} \approx 3$) giving way to an unsteady-transport balance, with corresponding upward growth of the turbulent layer, to match the edge imposed by our small, fixed values of E and ϵ in the freestream (this unsteadiness, however, has an imperceptible effect on the main region $\tilde{z} \lesssim 1.2$, which is in steady-state). This unsteady-transport region at the extreme top, shown by Cazalbou et al. (1994) as the correct balance at the edge of turbulent shear flows when the standard values are used, reflects the inability of the standard values to accommodate an edge at the top of the transport-dissipation region, since these give $\kappa \approx 2.5$ and hence laminarization of the region as $z \to \infty$ (Figure 1). In case K13 (Figure 6b), on the other hand, the transport-dissipation region laminarizes at a finite height ($\tilde{z} \approx 1$), consistent with analytical expectations for κ near one (Figure 1), and as such the region is much shallower and weakly turbulent (and hence less evident with the scaling used in figure) than that in case RO6. Behaviour with respect to laminarization of the transport-dissipation region in cases not shown is also consistent with analytical expectations.

Profiles of predicted l are shown in Figure 7. The analytical l behaviour is exhibited clearly in the upper NABL; for $\kappa > 2$ (RO6) there is monotonic increase

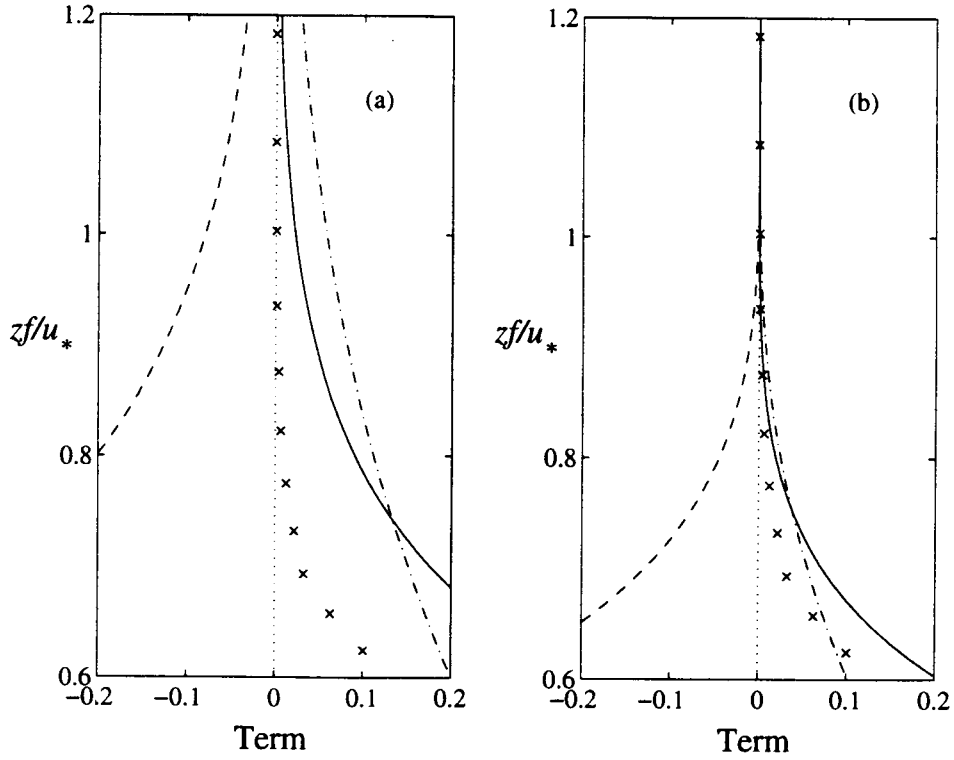

Figure 6. $E - \epsilon$ model profiles in the upper NABL of non-dimensional TKE budget terms for cases (a) RO6 and (b) K13. Shear production (solid), dissipation (dashed), transport (dashed-dot). C99 DNS data for shear production plotted as 'x'.

with height, for $\kappa = 2$ (K20) a constant value is reached, and for $\kappa < 2$ (K17-K10) values decrease with height. The kinks at the extreme top for cases K15-K10 are probably caused by course vertical resolution and/or coupling to freestream values of E and ϵ that are not exactly zero (as opposed to the upper boundary conditions of the PL-E solution, for which E and ϵ are exactly zero). Predicted E profiles (Figure 8) are also consistent with analytical expectations in tending towards laminarization at a finite height as κ decreases towards one.

To elaborate, we show in Figure 9 predictions of K_m and l for runs with κ equal to 2.5, 2.0 and 1.3, but with κ lowered in the latter two by changing the value of σ_ϵ (to 1.04 and 0.68, respectively) leaving $c_{\epsilon 2}$ and σ_e at their standard values. To maintain $k \approx 0.4$ in (9), $c_{\epsilon 1}$ was also lowered (to 1.41 and 1.14, respectively) in these cases. It is seen that profiles are practically identical to those in Figures 4 and 7 of identical κ, emphasizing that κ, rather than the parameters on an individual basis, controls predictions near the NABL top. It should be mentioned, however, that the lower values of $c_{\epsilon 1}$ used in these cases would give overly large growth rates of turbulence in neutrally-stratified free shear flows (Durbin and Pettersson-Reif,

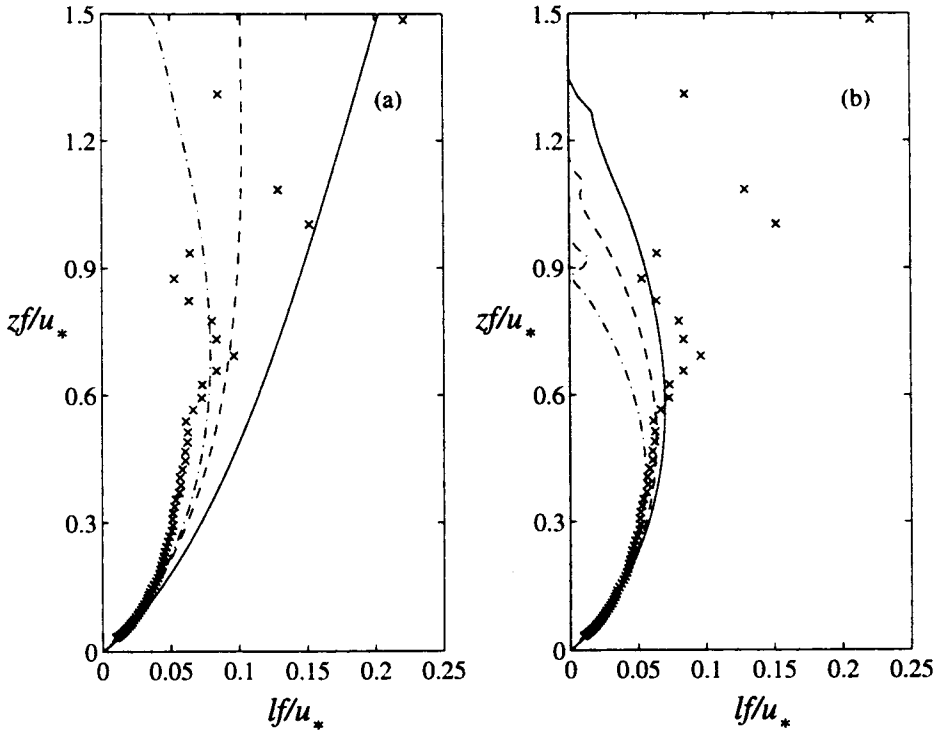

Figure 7. As in Figure 4, but for non-dimensional l.

2001). Lowering κ by raising σ_e (as done in cases K20-K10), on the other hand, would not sacrifice such predictive accuracy, since this necessitates no alteration to $c_{\epsilon 1}$.

A more extensive relevance check could include comparison of predicted E and ϵ profiles near the NABL top with appropriate (depending on κ) analytical solutions. We feel, however, that the exhibition in the numerical profiles of the central qualitative analytical features, the transport-dissipation balance near the NABL top, the transitional l behaviour at $\kappa = 2$, and the tendency of turbulence quantities towards laminarization at a finite height as $\kappa \to 1$, gives convincing evidence supporting relevance of the analytical solutions to the full model's near the NABL top.

Concerning accuracy, predictions of K_m (Figure 4) and l (Figure 7) within the bulk region $0.2 \lesssim \tilde{z} \lesssim 0.6$ (above which our deduced DNS profiles are not accurate) as well as of E up to the NABL top (Figure 8) are improved considerably as κ is lowered. Corresponding improvements are seen in predictions of $\tilde{h}_\tau$ (Table I). It is interesting that, although the direct effects of varying κ are on behaviour within the capping transport-dissipation region, predictive improvements of K_m and l are felt in the bulk region beneath, pointing to the importance of diffusional

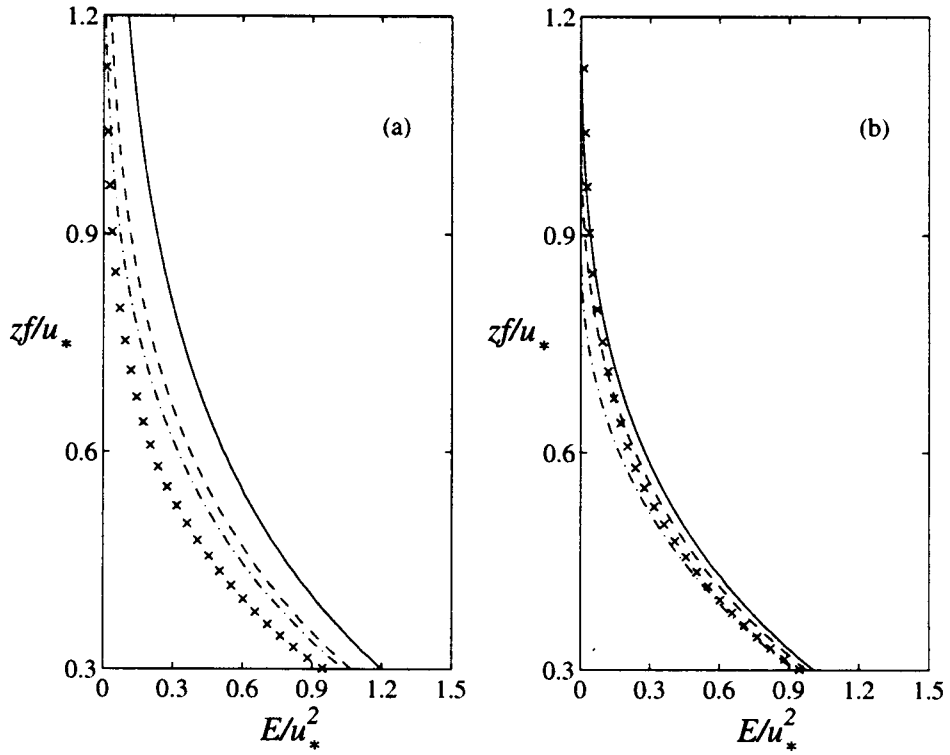

Figure 8. As in Figure 4, but for non-dimensional E in the region $0.3 \leq \tilde{z} \leq 1.2$.

coupling of the entire NABL to behaviour at the top. Best agreement is found for $\kappa = 1.3$, for which the analytical and numerical solutions produce an edge to the capping transport-dissipation region. An edge is also suggested in the DNS E profile (Figure 8), as is the corresponding transport-dissipation energy balance by the tendency towards zero with height of the DNS TKE shear production (Figure 6), leaving transport and dissipation as the only steady balance that can support the non-zero TKE found in the upper NABL. An edge to the transport-dissipation region thus appears a physical feature that necessitates accommodation in the $E-\epsilon$ model for accurate NABL prediction, and our numerical results suggest that this is adequately achieved by lowering κ from its standard value of ≈ 2.5 to ≈ 1.3. To maintain proper prediction of traditional engineering benchmark flows and to satisfy (9) with $k \approx 0.4$, we propose carrying this out by altering σ_ϵ and σ_e from their standard values to ≈ 1.1 and 1.6, respectively, maintaining standard values for the remaining parameters. It is seen (Figure 2, symbol '$*$') that surface drag predictions with $\kappa = 1.3$ are not significantly different than those computed in the standard cases, also the case (not shown) for mean velocity and turbulence profiles in the lower NABL. Model accuracy in the lower NABL is therefore not lost with $\kappa = 1.3$.

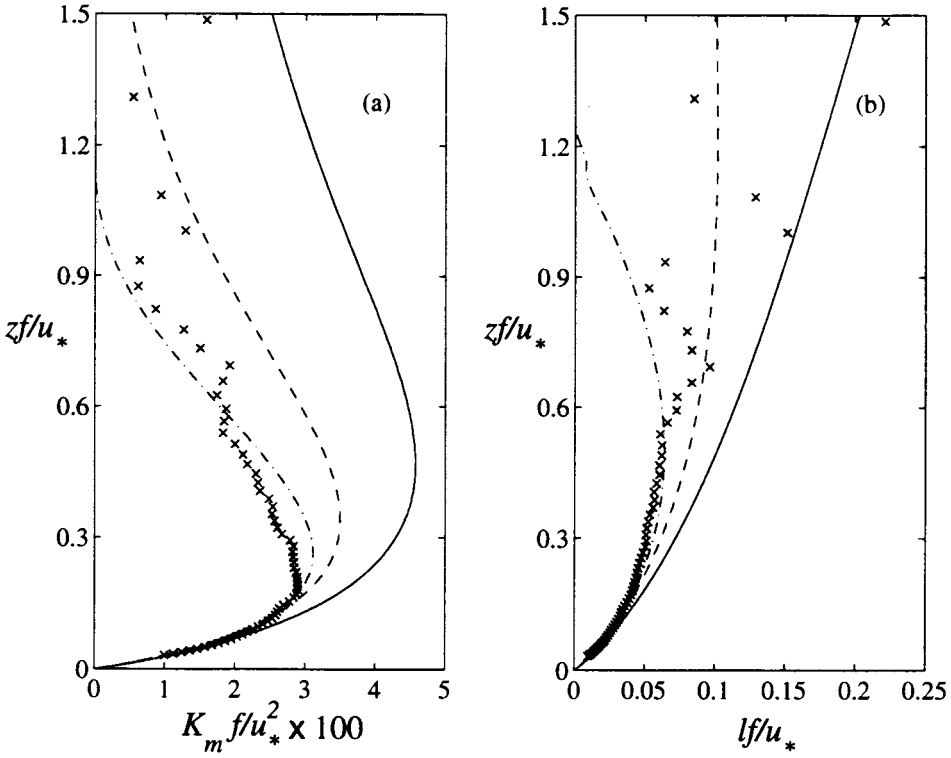

Figure 9. $E - \epsilon$ model predictions of non-dimensional a) K_m and b) l for cases with κ lowered by altering the value of σ_ϵ and leaving σ_e and $c_{\epsilon 2}$ at standard values. See text for further details. Solid, $\kappa = 2.5$; dashed, $\kappa = 2$; dashed-dot, $\kappa = 1.3$. C99 DNS data for $\tilde{z} > 0.03$ plotted as 'x'.

Finally, we revisit the underprediction of E in the lower NABL. As stated earlier, this is caused by an overly high value of β_0. In fact, it appears that $\beta_0 = c_\mu^{1/2}$ decreases with Reynolds number (Degraaff and Eaton, 2000), with atmospheric surface-layer observations (of very high Reynolds number) supporting $\beta_0 \approx 0.17$ (Panofsky et al., 1977; Kader and Yaglom, 1990). The E profile from a run with $c_\mu = 0.0289$ (corresponding to $\beta_0 = 0.17$) and $\sigma_\epsilon = 1.96$ and $\sigma_\epsilon = 2.89$ reset to give, assuming standard values of $c_{\epsilon 1}$ and $c_{\epsilon 2}$, $k = 0.4$ and $\kappa = 1.3$ is shown in Figure 5 (dashed line). The increase in E in the lower NABL is clear, and it is evident that agreement with the DNS would be obtained by choosing an appropriate value of c_μ between 0.0289 and 0.09 (with, of course, recalibration of σ_ϵ and σ_e). An edge to the E profile at the boundary-layer top is produced since $\kappa = 1.3$. Finally, predictions of surface drag as well as mean velocity and turbulence profiles (except, of course, for E) in the lower NABL for this case (not shown) are indistinguishable from those of the same Ro for $\kappa = 1.3$ and $c_\mu = 0.09$. The 'lower-c_μ' parameter values used in this run are therefore those giving optimal prediction of all variables in the NABL, while the ones we propose above (with $c_\mu = 0.09$) do not capture

the higher E in the lower NABL found in high Reynolds number field NABLs. The lower c_μ, however, is inconsistent with experimental data for equilibrium neutrally-stratified turbulent free shear layers, for which $c_\mu = 0.09$ is more appropriate (e.g., Tavoularis and Karnik, 1989).

5. Conclusion

$E - \epsilon$ model predictions of the neutrally-stratified atmospheric boundary layer (NABL) were reinvestigated to determine the cause for turbulence overpredictions found in previous applications. Analytical solutions for the case of steady transport-dissipation balance in the E and ϵ equations were derived to isolate possible model behaviour near the NABL top. It is found that closure parameter ratio $\kappa \equiv c_{\epsilon 2}\sigma_\epsilon/\sigma_e$ is the key control determining the type of analytical solution to the model's transport-dissipation problem. Although physical solutions exist for $1 \leq \kappa \leq 10/3$, solutions in which E and ϵ laminarize at a finite height necessitate a value of κ in the lower portion of this range, with laminarization as $z \to \infty$ for greater κ. The point $\kappa = 2$ is furthermore found as that where turbulent length scale (l) profiles transition from ones of decreasing ($\kappa < 2$) to increasing ($\kappa > 2$) values with height. Numerically computed profiles near the NABL top are consistent with analytical solutions. The height-increasing values of l predicted throughout the NABL with standard-valued parameters thus appear to result from $\kappa \approx 2.5$ (> 2), inferred from these values.

Comparison of numerical predictions with DNS data of Coleman (1999) concur with previous applications in finding turbulence overprediction in the middle and upper portion of the NABL when standard-valued parameters are used. Improved agreement, however, is obtained as κ is lowered towards one, with excellent agreement for $\kappa \approx 1.3$. Predictions are therefore improved as κ is lowered towards values producing laminarization of the capping transport-dissipation region at a finite height, a behaviour also suggested in DNS E profile. Accommodation in the $E - \epsilon$ model for laminarization thus seems necessary for accurate prediction of the NABL. To maintain consistency with pre-existing engineering flow constraints on the choice of parameter values, we propose to accommodate laminarization by resetting the values of closure parameters σ_ϵ and σ_e to ≈ 1.1 and 1.6, respectively, giving, with $c_{\epsilon 2} = 1.92$, $\kappa \approx 1.3$. The need for laminarization gives physical interpretation to the additional production term deemed necessary in (7) in previous applications for accurate prediction of the NABL.

Acknowledgements

The authors thank Dr. G. M. Coleman for supplying and discussing with us his DNS data, as well as Dr. P. A. Durbin and Dr. R. D. Bornstein for helpful comments regarding this work. The research was supported by grants from the National

Science Foundation and the National Aeronautics and Space Administration under the New Investigator Program (NIP) in Earth Sciences.

References

Andrén, A.: 1991, 'A TKE-Dissipation Model for the Atmospheric Boundary Layer', *Boundary-Layer Meteorol.* **56**, 207–221.

Apsley, D. D. and Castro, I. P.: 1997, 'A Limited-Length-Scale $k-\epsilon$ Model for the Neutral and Stably-Stratified Atmospheric Boundary Layer', *Boundary-Layer Meteorol.* **83**, 75–98.

Blackadar, A. K.: 1962, 'The Vertical Distribution of Wind and Turbulent Exchange in a Neutral Atmosphere', *J. Geophys. Res.* **67**, 3095–3102.

Briggs, D. A., Ferziger, J. H., Koseff, J. R., and Monismith, S. G.: 1996, 'Entrainment in a Shear-Free Turbulent Mixing Layer', *J. Fluid Mech.* **310**, 215–241.

Cazalbou, J. B., Spalart, P. R., and Bradshaw, P.: 1994, 'On the Behavior of Two-Equation Models at the Edge of a Turbulent Region', *Phys. Fluids* **6**, 1797–1804.

Coleman, G. M.: 1999, 'Similarity Statistics from a Direct Numerical Simulation of the Neutrally Stratified Planetary Boundary Layer', *J. Atmos. Sci.* **56**, 891–899.

Coleman, G. M., Ferziger, J. H., and Spalart, P. R.: 1990, 'A Numerical Study of the Turbulent Ekman Layer', *J. Fluid Mech.* **213**, 313–348.

Deaves, D. M.: 1981, 'A Note on the Upper Boundary Conditions for Turbulence Models in the Neutral Atmosphere', *Boundary-Layer Meteorol.* **21**, 489–493.

Degraaff, D. B. and Eaton, J. K.: 2000, 'Reynolds Number Scaling of the Flat Plate Turbulent Boundary Layer', *J. Fluid Mech.* **422**, 319–386.

Detering, H. W. and Etling, D.: 1985, 'Application of the $E-\epsilon$ Turbulence Model to the Atmospheric Boundary Layer', *Boundary-Layer Meteorol.* **33**, 113–133.

Durbin, P. A. and Pettersson-Reif, B. A.: 2001, *Statistical Theory and Modeling for Turbulent Flow*, John Wiley and Sons, Chichester, U.K., 285 pp.

Duynkerke, P. G.: 1988, 'Application of the $E-\epsilon$ Turbulence Closure Model to the Neutral and Stable Atmospheric Boundary Layer', *J. Atmos. Sci.* **45**, 865–880.

Garratt, J. R.: 1992, *The Atmospheric Boundary Layer*, Cambridge University Press, Cambridge, U.K., 316 pp.

Grant, A. L. M.: 1992, 'The Structure of Turbulence in the Near-Neutral Atmospheric Boundary Layer', *J. Atmos. Sci.* **49**, 226–239.

Huang, C. and Raman, S.: 1991, 'Numerical Simulation of January 28 Cold Air Outbreak during GALE: Part I: The Model and Sensitivity Tests of Turbulence Closures', *Boundary-Layer Meteorol.* **55**, 381–407.

Jones, W. P. and Launder, B. E.: 1972, 'The Prediction of Laminarization with a Two-Equation Model of Turbulence', *Int. J. Heat Fluid Flow* **15**, 301–314.

Kader, B. A. and Yaglom, A. M.: 1990, 'Mean Fields and Fluctuation Moments in Unstably Stratified Turbulent Boundary Layers', *J. Fluid Mech.* **212**, 637–662.

Koo, Y. and Reible, D. D.: 1995, 'Flow and Transport Modeling in the Sea-Breeze. Part I: A Modified $E-\epsilon$ Model with a Non-Equilibrium Level 2.5 Closure', *Boundary-Layer Meteorol.* **75**, 109–140.

Mason, P. J. and Thomson, D. J.: 1987, 'Large-Eddy Simulations of the Neutral Static-Stability Planetary Boundary Layer', *Quart. J. Roy. Meteorol. Soc.* **113**, 413–444.

Panofsky, H. A., Tennekes, H., Lenschow, D. H., and Wyngaard, J. C.: 1977, 'The Characteristics of Turbulent Velocity Components in the Surface Layer under Convective Conditions', *Boundary-Layer Meteorol.* **11**, 355–361.

Speziale, C. G. and Bernard, P. S.: 1992, 'The Energy Decay of Self-Preserving Isotropic Turbulence Revisited', *J. Fluid Mech.* **241**, 645–667.

Speziale, C. G. and Gatski, T. B.: 1996, 'Analysis and Modelling of Anisotropies in the Dissipation Rate of Turbulence', *J. Fluid Mech.* **344**, 155–180.

Tavoularis, S. and Karnik, U.: 1989, 'Further Experiments on the Evolution of Turbulent Stresses and Scales in Uniformly Sheared Turbulence', *J. Fluid Mech.* **204**, 457–478.

Tennekes, H. and Lumley, J. L.: 1972, *A First Course on Turbulence*, MIT, Cambridge, MA, 300 pp.

Wilcox, D. C.: 1998, *Turbulence Modeling for CFD*, DCW Industries Inc., La Canada, CA.

Xu, D. and Taylor, P. A.: 1997, 'An $E - \epsilon$-l Turbulence Closure Scheme for Planetary Boundary Layer Models: The Neutrally Stratified Case', *Boundary-Layer Meteorol.* **84**, 247–266.